Simultaneous estimation of phase behavior and second-derivative properties using the statistical associating fluid theory with variable range approach

Cite as: J. Chem. Phys. **124**, 024509 (2006); https://doi.org/10.1063/1.2140276
Submitted: 02 June 2005 . Accepted: 27 October 2005 . Published Online: 12 January 2006

Thomas Lafitte, David Bessieres, Manuel M. Piñeiro, and Jean-Luc Daridon

Simultaneous estimation of phase behavior and second-derivative properties using the statistical associating fluid theory with variable range approach

Thomas Lafitte[a] and David Bessieres
Laboratoire des Fluides Complexes, Groupe Haute Pression, Université de Pau et des Pays de l'Adour, B.P. 1155, 64013 Pau Cedex, France

Manuel M. Piñeiro
Departamento de Física Aplicada, Facultade de Ciencias, Universidade de Vigo, E-36310 Vigo, Spain

Jean-Luc Daridon
Laboratoire des Fluides Complexes, Groupe Haute Pression, Université de Pau et des Pays de l'Adour, B.P. 1155, 64013 Pau Cedex, France

(Received 2 June 2005; accepted 27 October 2005; published online 12 January 2006)

A modified statistical associating fluid theory (SAFT) with variable range version is presented using the family of *m*-*n* Mie potentials. The use of this intermolecular potential for modeling repulsion-dispersion interactions between the monomer segments, together with a new method for optimizing the molecular parameters of the equation of state, is found to give a very accurate description of both vapor-liquid equilibria and compressed liquid bulk properties (volumetric and derivative properties) for long-chain *n*-alkanes. This new equation improves other SAFT-like equations of state which fail to describe derivative properties such as the isothermal compressibility and the speed of sound in the condensed liquid phase. Emphasis is placed on pointing out that the key for modeling the latter properties is the use of a variable repulsive term in the intermolecular potential. In the case of the *n*-alkanes series, a clear dependence of the characteristic molecular parameters on increasing chain length is obtained, demonstrating their sound physical meaning and the consistency of the new fitting procedure proposed. This systematic method for optimizing the model parameters includes data on the saturation line as well as densities and speed of sound data in the condensed liquid phase, and the results show undoubtedly that the model performance is enhanced and its range of applicability is now widened, keeping in any case a good balance between the accuracy of the different estimated properties. © *2006 American Institute of Physics*. [DOI: 10.1063/1.2140276]

I. INTRODUCTION

Both design and efficient cost running of industrial processes involving fluids rely on the possibility of having an accurate simultaneous description of phase equilibria and thermophysical properties of the pure fluids and mixtures involved. For instance, in the oil and gas industries, special attention is devoted to the recovery of the heavy crude oil. In this particular case, extremely complex multiphase mixtures are present, containing molecules of very different shapes, sizes, and structures. Most classical equations of state (EOS), with a formulation based on the assumption that molecules can be considered nearly spherical, prove to be inaccurate when they are applied to complex molecules. In addition to this inadequacy, the characteristic parameters that must be fitted in each case are usually tuned almost exclusively to phase equilibrium data in order to obtain the best representation possible of vapor-liquid equilibrium. This property is undoubtedly of primary interest for practical purposes, but calculating fitting parameters this way usually yields poor estimations of other properties as, for instance, compressed liquid bulk properties. Moreover, if the parameters calculated using this classical approach are used to extend estimations to second-derivative properties (isobaric heat capacity, speed of sound, thermal expansivity or compressibility) deviations from real behavior reach limits that make results useless. The contrary also applies: estimations obtained from parameters fitted on thermophysical properties show poor agreement with experimental phase equilibrium. Related to this fact, it is widely agreed that estimation of second-derivative properties is one of the most demanding tests to check the performance limits for a thermodynamic model or equation. Dedicated EOS are widely used for some substances, but the large number of parameters involved does not allow making any guess on the physics behind the model despite their good performance. The parameters are not transferable and little positive knowledge can be extrapolated to describe other similar substances; these approaches remain effectively as correlations of large databases. Thus, the detailed study of EOS offering a formulation versatile enough to describe simultaneously phase equilibrium and first- and second-derivative fluid properties with acceptable accuracy remains an open problem. Another closely related question is, as mentioned before, the determination of a systematic method

[a]Electronic mail: t.lafitte@etud.univ-pau.fr

to combine experimental data of different properties to calculate reliable characteristic parameters that can draw the maximum performance of the theory keeping a balance between accuracies.

Over the last few years, the popularity of the statistical associating fluid theory[1] (SAFT)-like EOS, based on a perturbation theory for associating fluids proposed by Wertheim,[2–7] has grown very fast. Nowadays this theoretical approach is very popular due to its versatility and the good results obtained in different applications. Müller and Gubbins[8] have recently published a comprehensive description of the theory and a list of successful applications, among which multiphase equilibrium of complex behavior molecules such as highly associating compounds, surfactants, micelles, asphaltenes, and polymers may be outlined. Nevertheless, the application of SAFT to second-derivative properties estimation has not yet been studied in detail, and contributions in this line are necessary to expand the range of applicability of the theory and determine precisely its real performance.

In this work, a modified version of the statistical associating fluid theory with variable range (SAFT-VR) model, combined with the family of *m*-*n* Mie potentials,[9] is presented. This approach has been applied to describe the behavior of linear alkanes from methane to *n*-hexatriacontane. The motivation for the election of alkanes is twofold. First, this family of fluids plays an essential role in many technical applications as, for instance, in the oil industry. Second, it is a homologous series of fluids that has been extensively studied, so reliable experimental data can be found for derived properties over wide pressure and temperature ranges. This fact allows performing a comprehensive study on the thermophysical influence of chain length. After preliminary tests on derivative properties of *n*-alkanes, with the perturbed-chain statistical associating fluid theory (PC-SAFT),[10] SAFT-VR for square-well potentials,[11] and SAFT-VR for Lennard-Jones chains,[12] poor results were obtained for the prediction of isothermal compressibilities of heavy *n*-alkanes. However, we should note at this point that the SAFT-VRX (Ref. 13) equation (a combination of the original SAFT-VR equation with a crossover technique developed by Kiselev[14] which satisfies the asymptotic critical power laws observed in real fluids, as well as the regular thermodynamic behavior far from the critical point) was successfully used by McCabe and Kiselev[15] to describe the high-pressure volumetric behavior of *n*-hexane. Nevertheless, since it turns out that the difficulty to model the second-derivative properties with classical SAFT-like EOS is observed over the whole pressure and temperature ranges and not only in the vicinity of the critical point, it seems that the solution to this second-derivative property estimation should be obtained by studying the original, analytical formulation, and hence, the potential interactions.

The SAFT-VR model was then modified in the framework of the theory proposed by Davies *et al.*[12] to account for soft repulsion in the intermolecular potential. In addition to this, instead of restricting the approach for the particular case of the Lennard-Jones (6,12) potential, the equation of state has been adapted to deal with any values of the exponents *m* and *n*. This was done by using the cavity function of the hard-core Mie potentials from the Barker and Henderson perturbation theory[16–18] together with an evaluation of the hard-core temperature-dependent diameter[18] using numerical integrations. Thus, an equation of state for variable repulsive and attractive ranges is obtained. The exponent of the attractive term was fixed, $m=6$, while the repulsive exponent n was considered as an extra adjustable pure-component parameter. The number of spherical segments can be linked to the number of carbon atoms, leaving only three parameters of the model to be adjusted. A new fitting procedure is proposed in order to improve the optimization, using data on four different properties: vapor pressure curve, saturated liquid densities, and densities and speed of sound data of the condensed liquid phase. A Levenberg-Marquadt[19] algorithm is applied for minimizing the objective function. Significant improvement is obtained using the SAFT-VR equation of state in its revised version for the estimation of all volumetric and derivative properties over wide pressure and temperature conditions without any deterioration of the vapor-liquid coexistence curve. The speed of sound, generally presented as a severe consistency test for EOS, was estimated with percent average absolute deviations [AAD (%) hereafter], close to 2% for the complete *n*-alkanes series up to *n*-hexatriacontane. As an example, the AAD (%) for speed of sound estimations is 2.75% for C_{36} instead of 10.2% using the SAFT-VR for square-well potentials.[11] Moreover, a clear dependence of the parameters on the number of carbon atoms is obtained, emphasizing the consistency of this new method and the physical meaning of the variable repulsive part in the intermolecular potential.

TABLE I. SAFT-VR LJC molecular parameters of some molecules of the *n*-alkanes series.

Substance	m_s	σ (Å)	(ε/k) (K)
C_6H_{14}	2.67	3.9622	257.46
C_7H1_6	3	3.9759	261.42
$C_{13}H_{28}$	5	4.0132	274.02
$C_{14}H_{30}$	5.33	4.0144	274.96
$C_{15}H_{32}$	5.67	4.0168	275.19
$C_{17}H_{36}$	6.33	4.0366	277.83

II. PRELIMINARY RESULTS

In order to evaluate the performance of the SAFT to model derivative properties of heavy *n*-alkanes, a comparative test between several versions of the theory has been performed. These versions were PC-SAFT (Ref. 10) and SAFT-VR (Ref. 11) for square-well potentials (SAFT-VR SW), together with an equation based on the SAFT-VR approach developed to deal with chains of Lennard-Jones[12] segments (SAFT-VR LJC). These EOSs have proven to describe accurately vapor pressures and saturated liquid densities of long-chain molecules. Despite this, their ability to correlate derivative properties has not been examined yet.

In previous studies, the characteristic parameters for the *n*-alkanes series for PC-SAFT (Ref. 10) and SAFT-VR SW (Ref. 20) were fitted to experimental vapor pressures and

TABLE II. Isothermal compressibility (β_T) of some *n*-alkanes in the condensed liquid phase. Comparison of experimental data with the calculation results of SAFT-VR SW (Ref. 11) [with the parameters derived by McCabe and Jackson (Ref. 20)], PC-SAFT (Ref. 10) [with the parameters derived by Gross and Sadowski (Ref. 10)], Soave-Redlich-Kwong (SRK), Peng-Robinson (PR), Lee-Kesler (LK), and Nishiumi-Saïto (NS).

	AAD (%), $\beta_T(T,P)$							
Substance	SRK	PR	LK	NS	PC-SAFT	SAFT-VR SW	SAFT-VR LJC	Reference
C_6H_{14}	26.1	25.7	5.4	13.4	22.5	12.3	29.8	32
$C_{15}H_{32}$	38.8	42.6	25.8	21.9	35.4	32.4	54.0	33
$C_{17}H_{36}$	43.7	49.3	20.5	30.1	36.8	29.8	57.0	33

saturated liquid densities. In the case of SAFT-VR LJC, the model parameter values are not available in literature. These parameters are the number of Lennard-Jones segments in the chain, m_s, the diameter of each segiment, σ, and the depth of the attractive part of the potential ε/k, and they were calculated here using the same fitting procedure. Their values for several *n*-alkanes are listed in Table I. It is important to note that since these parameters are supposed to be physically meaningful, they could be used directly to estimate other properties, such as isobaric heat capacities, isothermal compressibilities, or speed of sound, either in equilibrium or in compressed fluid conditions. With this objective, we applied PC-SAFT,[10] SAFT-VR SW,[11] and SAFT-VR LJC (Ref. 12) (the latter with the parameters calculated here) to estimate these derivative properties. The main objective of this preliminary calculation was not an exhaustive investigation of all the derivative properties for *n*-alkanes, but to identify the limitations of the equations. As a result, a common deficiency of these three versions in estimating the isothermal compressibility (β_T) of heavy *n*-alkanes in the condensed liquid phase was observed. This is shown in Table II, where the estimation results of these three versions for some *n*-alkanes from *n*-hexane (C_6) to *n*-heptadecane (C_{17}) are listed. In order to have more references of the accuracy of different EOSs dealing with the same problem, the deviations obtained with two classical cubic equations, Peng-Robinson[21] (PR) and Soave-Redlich-Kwong[22] (SRK), as well as two models based on the Benedict-Webb-Rubin[23] approach, Lee Kesler[24] (LK) and Nishiumi-Saïto[25] (NS), are also listed.

These results show that even though SAFT equations [PC-SAFT (Ref. 10), and SAFT-VR SW (Ref. 11)] give a slightly better prediction for the speed of sound than that calculated with cubic EOS, a significant deterioration is soon found with increasing chain length. Regarding Lee-Kesler[24] and Nishiumi-Saïto,[25] which are supposed to be the most reliable models in this context since they involve a large number of parameters adjusted exclusively on the compressed liquid bulk properties, they also produce poor results for heavy *n*-alkanes.

As a consequence, and due to the fact that the isothermal compressibility is the predominant term in the calculation of the speed of sound (u), all these equations completely fail to describe this property (see Table III).

To overcome this problem, a feasible solution might be to recalculate molecular parameters for PC-SAFT,[10] SAFT-VR SW,[11] and SAFT-VR LJC (Ref. 12) by taking into consideration isothermal compressibility data (or speed of sound data) in the fitting procedure (this is described in detail in Sec. IV A). This test was checked, but a slight improvement on β_T estimation results induced an important deterioration of the vapor-liquid equilibrium curve. Thus, assuming that the SAFT theory contains the correct physics to model these derivative properties induces one to think that the deficiencies described above are due to the choice of the intermolecular potential used to model the repulsion-dispersion interactions involved in *n*-alkanes. These are the modified square-well potential [PC-SAFT (Ref. 10)], the square-well potential of variable attractive range [SAFT-VR SW (Ref. 11)], and the Lennard-Jones potential [SAFT-VR LJC (Ref. 12)]. Therefore, our goal in the next section is to find an intermolecular potential model suitable for describing both vapor-liquid equilibrium and condensed liquid-phase properties.

TABLE III. Speed of sound (u) of some *n*-alkanes in the condensed liquid phase. Comparison of experimental data with the calculation results of SAFT-VR SW (Ref. 11) [with the parameters derived by McCabe and Jackson (Ref. 20)], PC-SAFT (Ref. 10) [with the parameters derived by Gross and Sadowski (Ref. 10)], Soave-Redlich-Kwong (SRK), Peng-Robinson (PR), Lee-Kesler (LK), and Nishiumi-Saïto (NS).

	AAD (%), $u(T,P)$							
Substance	SRK	PR	LK	NS	PC-SAFT	SAFT-VR SW	SAFT-VR LJC	Reference
C_6H_{14}	14.1	13	0.8	6.9	10.3	4.7	15.9	32
C_7H_{16}	16.4	15.7	2.1	8.5	11.4	6.5	17.7	34
$C_{13}H_{28}$	38.2	38.7	11	12.8	15.4	11.4	22.7	35
$C_{14}H_{30}$	38.6	38.5	12.6	10.7	16.0	18.2	23.0	35
$C_{15}H_{32}$	38.1	38.3	14.7	11.3	16.1	12.6	23.3	33
$C_{17}H_{36}$	46.7	47.5	15.9	13.1	16.6	12.2	23.6	33

III. SAFT-VR MIE EQUATION OF STATE

The residual Helmholtz free energy for associating chain molecules is described in the SAFT approach as

$$\frac{A^{\text{res}}}{NkT} = \frac{A^{\text{mono}}}{NkT} + \frac{A^{\text{chain}}}{NkT} + \frac{A^{\text{assoc}}}{NkT}, \tag{1}$$

where N is the number of molecules, T is the temperature, and k is the Boltzmann constant. In this equation A^{mono},A^{chain}, and A^{assoc} are the contributions from the monomer segments (M), the formation of chains, and the existence of intermolecular association, respectively.

Gil-Villegas *et al.*[11] showed in previous works that the SAFT-VR approach could be used to deal with homonuclear chains of hard-sphere segments of equal diameter σ interacting via different intermolecular potentials such as the square well, Sutherland, or Yukawa potentials. In all cases, the intermolecular potential can be written as follows:

$$u^M(r) = u^{\text{hs}}(r,\sigma) - \varepsilon\phi(r,\lambda), \tag{2}$$

where u^{hs} is the hard-sphere repulsive interaction and $-\varepsilon\phi(r,\lambda)$ is the attractive part of range λ and depth $-\varepsilon$.

In these SAFT-like equations of state the variable λ is taken as a parameter for controlling the potential range. The approach is then very general and allows studying chain molecules formed from hard-core monomers with an arbitrary potential of variable attractive range. However, further extensions of the SAFT-VR theory have been proposed to account for chain molecules formed by soft-core segments. Davies *et al.*[12] proposed, for instance, a version of the SAFT-VR equation of state adapted to the generalized Mie[9] *m-n* potential, but results were only shown for the particular case of the SAFT-VR LJC. A comparison with the expression of Johnson *et al.*[26] has been made and comparable accuracy was found far from the critical region. Nevertheless, it is important to note here that when the equation is used in the particular case of the Lennard-Jones potential, the "variable range" aspect of the theory is lost. Thus, in this section an alternative is proposed, allowing the application of the theory for any pair of *m-n* values; that is, establishing the possibility to vary the range of both the repulsive and attractive terms of the intermolecular potential.

A. The Mie potentials

The Mie[9] potentials (λ_2,λ_1) are given by

$$u^M = C\varepsilon\left[\left(\frac{\sigma}{r}\right)^{\lambda_2} - \left(\frac{\sigma}{r}\right)^{\lambda_1}\right], \tag{3}$$

where

$$C = \frac{\lambda_2}{\lambda_2-\lambda_1}\left(\frac{\lambda_2}{\lambda_1}\right)^{\lambda_1/(\lambda_2-\lambda_1)}. \tag{4}$$

The Barker and Henderson (BH) perturbation theory[18] demonstrated that systems interacting with binary potentials with soft repulsive interactions could be described by considering an equivalent potential with a hard-core temperature-dependent diameter:

$$u^M_{\text{BH}} = \begin{cases} \infty & \text{if } r < \sigma_{\text{BH}}(T) \\ u^M & \text{if } r > \sigma_{\text{BH}}(T) \end{cases}, \tag{5}$$

where

$$\sigma_{\text{BH}}(T) = \int_0^\sigma \left(1 - \exp\left(\frac{-u^M}{kT}\right)\right)dr. \tag{6}$$

The intermolecular potential u^M_{bH} can then be written as follows:

$$u^M_{\text{BH}} = u^{\text{hs}}(r,\sigma_{\text{BH}}) - \varepsilon\phi^M(r;\sigma_{\text{BH}},\lambda_1,\lambda_2), \tag{7}$$

with

$$u^{\text{hs}}(r,\sigma_{\text{BH}}) = \begin{cases} \infty & \text{if } r < \sigma_{\text{BH}} \\ 0 & \text{if } r > \sigma_{\text{BH}} \end{cases} \tag{8}$$

and

$$\phi^M(r,\sigma_{\text{BH}},\lambda_1,\lambda_2) = C[\phi^S(r,\sigma_{\text{BH}},\lambda_1) - \phi^S(r,\sigma_{\text{BH}},\lambda_2)]. \tag{9}$$

$\phi^S(r,\sigma_{\text{BH}},\lambda)$ stands for the shape of the generalized Sutherland potential for hard spheres of diameter σ_{BH}:

$$\phi^S(r,\sigma_{\text{BH}},\lambda) = (\sigma_{\text{BH}}/r)^\lambda. \tag{10}$$

The Mie potentials *m-n* (Ref. 9) are then obtained by substituting $\lambda_1=m$ and $\lambda_2=n$.

B. Monomer contribution

In this section we recall the analytical expressions developed by Gil-Villegas *et al.*[11] that lead to an equation of state for segments interacting via the Mie[9] potential.

For pure components the monomer Helmholtz free energy can be expressed as

$$\frac{A^{\text{mono}}}{NkT} = m_s\frac{A^M}{N_skT} = m_sa^M, \tag{11}$$

where m_s is the number of segments in the chain, N_s is the total number of spherical segments, and $a^M=A^M/N_skT$ is the excess Helmholtz free energy per monomer segment. Applying the high-temperature expansion given by the Barker-Henderson[18] theory for hard-core systems to a^M, the following expression is obtained:

$$a^M = a^{\text{hs}} + \beta a_1^M + \beta^2 a_2^M, \tag{12}$$

where $\beta=1/kT$, a^{hs} is the residual free energy of a system of hard spheres of diameter σ_{BH}, and a_1^M and a_2^M are the first two perturbation terms[18] associated with the attractive term of the potential.

The expression of Carnahan and Starling[27] is used for the hard-sphere residual free energy,

$$a^{\text{hs}} = \frac{4\eta_{\text{BH}} - 3\eta_{\text{BH}}^2}{(1-\eta_{\text{BH}})^2}, \tag{13}$$

where $\eta_{\text{BH}}=\pi\sigma_{\text{BH}}^3\rho_s/6$ is the packing fraction of the system and $\rho_s=N_s/V$ is the monomer density.

The first perturbation term a_1^{Mie} is given by[18]

$$a_1^M = -2\pi\rho_s\varepsilon\int_{\sigma_{BH}}^{\infty} r^2\phi^M(r)g^{hs}(r)dr, \tag{14}$$

where g^{hs} stands for the radial distribution function of the hard-sphere system. This expression can be expanded using Eq. (8):

$$a_1^M = -2\pi\rho_s\varepsilon C\int_{\sigma_{BH}}^{\infty} r^2\phi^{S\lambda_1}(r)g^{hs}(r)dr + 2\pi\rho_s\varepsilon C\int_{\sigma_{BH}}^{\infty} r^2\phi^{S\lambda_2}(r)g^{hs}(r)dr. \tag{15}$$

Thus, the mean attractive energy can be expressed as

$$a_1^M = C[-a_1^S(\eta_{BH},\lambda_2) + a_1^S(\eta_{BH},\lambda_1)], \tag{16}$$

where a_1^s corresponds to the mean attractive energy for a Sutherland-λ system, but evaluated with the effective packing fraction.

Using the mean-value theorem, Gil-Villegas *et al.*[11] obtained an analytical expression for powers in the range $3 < \lambda \leq 12$:

$$a_1^S(\eta_{BH},\lambda) = a_1^{VDW}(\eta_{BH},\lambda)g^{hs}(1,\eta_{eff}(\eta_{BH})), \tag{17}$$

where

$$a_1^{VDW}(\eta_{BH};\lambda) = -4\eta_{BH}\varepsilon\left(\frac{3}{\lambda-3}\right) \tag{18}$$

and

$$g^{hs}(1;\eta_{eff}) = \frac{1-\eta_{eff}/2}{(1-\eta_{eff})^3}. \tag{19}$$

η_{eff} is an effective packing fraction defined by

$$\eta_{eff}(\eta;\lambda) = c_1\eta_{BH} + c_2\eta_{BH}^2, \tag{20}$$

with

$$\begin{pmatrix} c_1 \\ c_2 \end{pmatrix} = \begin{pmatrix} -0.943\,973 & 0.422\,543 & -0.037\,176\,3 & 0.001\,169\,01 \\ 0.370\,942 & -0.173\,333 & 0.017\,559\,9 & -0.000\,572\,729 \end{pmatrix}\begin{pmatrix} 1 \\ \lambda \\ \lambda^2 \\ \lambda^3 \end{pmatrix}. \tag{21}$$

The second-order perturbation term a_2^{Mie} is evaluated using the local compressibility approximation[18] (LCA):

$$a_2^M = \frac{1}{2}\varepsilon K^{hs}\eta_{BH}\frac{\partial a_1^{M^*}}{\partial_{BH}}, \tag{22}$$

where K^{hs} is the Percus-Yevick[28] hard-sphere isothermal compressibility,

$$K^{hs} = \frac{(1-\eta_{BH})^4}{1+4\eta_{BH}+4\eta_{BH}^2}. \tag{23}$$

For the Mie[9] potentials,

$$a_1^{M^*} = C[-a_1^S(\eta_{BH},2\lambda_2) + a_1^S(\eta_{BH},2\lambda_1)]. \tag{24}$$

The following expression is then obtained:

$$a_2^M = \frac{C}{2}\varepsilon K^{hs}\eta_{BH}\frac{\partial}{\partial\eta_{BH}}[-a_1^S(\eta_{BH},2\lambda_2) + a_1^S(\eta_{BH},2\lambda_1)]. \tag{25}$$

Gil-Villegas *et al.*[11] assumed that if the condition $\lambda_2 > 6$ is imposed, the second-order term, corresponding to the fluctuation of the total energy, is then obtained in terms only of the attractive contribution as

$$a_2^M = \frac{C}{2}\varepsilon K^{hs}\eta_{BH}\frac{\partial a_1^s(\eta_{BH},2\lambda_1)}{\partial\eta_{BH}}. \tag{26}$$

C. Chain contribution

In the original SAFT-VR EOS for (SAFT-VR LJC), Davies *et al.*[12] made an approximation for the evaluation of the chain term using the cavity function of a Sutherland-6 system instead of the cavity function of the hard-core LJ potential from the Barker-Henderson theory.[18] Indeed, it appeared that the latter function provided a less accurate description of the thermodynamic properties of the Lennard-Jones chains. Despite this, as we are interested here in the general case of the Mie[9] potentials family, it is highly probable that the approximation proposed for the specific case of the Lennard-Jones system might not be fully satisfactory for a generalized *m-n* potential. Therefore, an analytical expression for the cavity function of the hard-core Mie potentials is proposed here. This is done in the framework of the theory of Gil-Villegas *et al.*[11] by applying the Clausius virial theorem together with the density derivative of the Helmholtz free energy. The expression for the contribution to the formation of a chain of m_s monomers is expressed as a function of the contact value of the monomer background correlation function:

$$\frac{A_{chain}}{NkT} = -(m_s-1)\ln y_b^M, \tag{27}$$

where y_b^M is the cavity function of the reference fluid for the interaction of two segments evaluated at the bond distance σ_{BH}.

For hard-core potentials the compressibility $Z^M = PV/N_s kT$ is given by

$$Z^M = 1 + \frac{2\pi}{3}\rho_s \int_0^\infty \frac{d}{dr}[\exp(-\beta u_{\mathrm{BH}}^M)]r^3 y^M(r)dr, \tag{28}$$

where $y^M = g^M(r)\exp(\beta u_{\mathrm{BH}}^M)$ is a continuous function. Since the derivative of $\exp(-\beta u_{\mathrm{BH}}^M)$ for $r < \sigma_{\mathrm{BH}}$ is a δ function of $(r-\sigma_{\mathrm{BH}})$, we obtain

$$\begin{aligned} Z^M &= 1 + \frac{2\pi\sigma_{\mathrm{BH}}^3}{3}\rho_S g^{\mathrm{hs}}(\sigma_{\mathrm{BH}}) \\ &\quad + \frac{2\pi}{3}\rho_S \int_{\sigma_{\mathrm{BH}}^+}^\infty \frac{d}{dr}[\exp(-\beta u_{\mathrm{BH}}^M)]r^3 y^M(r)dr \\ &= Z^{\mathrm{hs}} + \frac{2\pi}{3}\rho_S \int_{\sigma_{\mathrm{BH}}^+}^\infty \frac{d}{dr}[\exp(-\beta u_{\mathrm{BH}}^M)]r^3 y^M(r)dr, \end{aligned} \tag{29}$$

where Z^{hs} represents the compressibility factor of a hard-sphere fluid.

As for the free energy, a high-temperature expansion[18] can be used at this point for the radial distribution function:

$$g^M(r) = g^{\mathrm{hs}}(r) + \beta\varepsilon g_1(r) + (\beta\varepsilon)^2 g_2(r) + \cdots. \tag{30}$$

Using this new expression for the radial distribution function, Eq. (30) can be written as follows:

$$\begin{aligned} Z^M &= Z^{\mathrm{hs}} + \frac{2\pi\sigma_{\mathrm{BH}}^3}{3}\rho_S \beta\varepsilon g_1^M(\sigma_{\mathrm{BH}}) \\ &\quad + \frac{2\pi}{3}\beta\varepsilon\rho_S \int_{\sigma_{\mathrm{BH}}^+}^\infty \frac{d}{dr}[\phi^M]r^3 g^{\mathrm{hs}}(r)dr + \cdots. \end{aligned} \tag{31}$$

An alternative way to express the compressibility factor is to use the high-temperature expansion of the Helmholtz function:

$$Z^M \frac{PV}{N_S kT} = -\frac{V}{N_S kT}\frac{\partial A^M}{\partial V} = \eta_{\mathrm{BH}}\frac{\partial a^M}{\partial \eta_{\mathrm{BH}}}. \tag{32}$$

Thus, using the expression for a^M given by Eq. (12), a second expression for the radial distribution function is obtained:

$$Z^M = Z^{\mathrm{hs}} + \beta\eta_{\mathrm{BH}}\frac{\partial a_1^M}{\partial \eta_{\mathrm{BH}}} + \beta^2\eta_{\mathrm{BH}}\frac{\partial a_2^M}{\partial \eta_{\mathrm{BH}}}. \tag{33}$$

Consequently, the combination of Eqs. (31) and (33) provides a simple analytical expression for $g_1(\sigma_{\mathrm{BH}})$:

$$g_1(\sigma_{\mathrm{BH}}) = \frac{1}{4\varepsilon}\frac{\partial a_1^M}{\partial \eta_{\mathrm{BH}}} - \frac{1}{\sigma_{\mathrm{BH}}^3}\int_{\sigma_{\mathrm{BH}}^+}^\infty \frac{d}{dr}[\phi^M]r^3 g^{\mathrm{hs}}(r)dr. \tag{34}$$

It is important to underline here that the calculation of $g_2(\sigma_{\mathrm{BH}})$ would have required a third-order expansion of the free energy. However, at this point it has been assumed that an expansion up to first order for the radial distribution function gives a good description of the properties of the Mie potentials.

Since the Mie[9] potentials can be expressed as a sum of two Sutherland potentials, the following expression applies:

$$\begin{aligned} g_1(\sigma_{\mathrm{BH}}) &= \frac{1}{4\varepsilon}\frac{\partial a_1^M}{\partial \eta_{\mathrm{BH}}} - \frac{C}{\sigma_{\mathrm{BH}}^3}\left[\int_{\sigma_{\mathrm{BH}}^+}^\infty \frac{d}{dr}[\phi^S(\lambda_1)]r^3 g^{\mathrm{hs}}(r)dr \right. \\ &\quad \left. - \int_{\sigma_{\mathrm{BH}}^+}^\infty \frac{d}{dr}[\phi^S(\lambda_2)]r^3 g^{\mathrm{hs}}(r)dr\right] \\ &= \frac{1}{4\varepsilon}\frac{\partial a_1^M}{\partial \eta_{\mathrm{BH}}} - \frac{C}{\sigma_{\mathrm{BH}}^3}\left[-\lambda_1\int_{\sigma_{\mathrm{BH}}^+}^\infty \phi^S(\lambda_1)r^2 g^{\mathrm{hs}}(r)dr \right. \\ &\quad \left. + \lambda_2\int_{\sigma_{\mathrm{BH}}^+}^\infty \phi^S(\lambda_2)r^2 g^{\mathrm{hs}}(r)dr\right]. \end{aligned} \tag{35}$$

On the right-hand side we recognize the expressions of the mean attractive energy of the Sutherland potentials. Equation (34) can then be written as

$$g_1(\sigma_{\mathrm{BH}}) = \frac{1}{4\varepsilon}\frac{\partial a_1^M}{\partial \eta_{\mathrm{BH}}} - \frac{C}{12\eta_{\mathrm{BH}}\varepsilon}[\lambda_1, a_1^S(\lambda_1) - \lambda_2 a_2^S(\lambda_2)]. \tag{36}$$

And finally, according to Eq. (32)

$$\begin{aligned} g^M(\sigma_{\mathrm{BH}}) &= g^{\mathrm{hs}}(\sigma_{\mathrm{BH}}) + \frac{1}{4}\beta\left[\frac{\partial a_1^M}{\partial \eta_{\mathrm{BH}}} - \frac{C\lambda_1}{4\eta_{\mathrm{BH}}}a_1^S(\lambda_1)\right. \\ &\quad \left. + \frac{C\lambda_2}{4\eta_{\mathrm{BH}}}a_2^S(\lambda_2)\right], \end{aligned} \tag{37}$$

where

$$y^M(\sigma_{\mathrm{BH}}) = g^M(\sigma_{\mathrm{BH}}). \tag{38}$$

By including this analytical expression for $y^M(\sigma_{\mathrm{BH}})$ in Eq. (27), a formal expression for an equation of state for nonassociating chains of spherical segments interacting through Mie[9] potentials is obtained.

Nevertheless, a difficulty remains in the evaluation of the temperature-dependent diameter of the segments σ_{BH} for any set of *m*-*n* values. It is clear that the calculation of the properties of these potentials will be very sensitive to the determination of the integral in Eq. (6), which is the basis of the calculation of all the terms in the equation of state. Since σ_{BH} depends on temperature but not on density, a solution could be to parametrize this diameter with an empirical equation in terms of $T^*(T^* = Tk/\varepsilon)$, as proposed by Gil-Villegas *et al.*[11] for the case of Lennard-Jones potential. However, extreme care must be taken when taking derivatives of equations with no physical meaning. Taking this into account, this method will be inadequate if the objective is the determination of properties involving σ_{BH} temperature derivatives (enthalpies, isobaric thermal expansivities, isobaric heat capacities, etc.). For this reason, the solution we advocate here is to evaluate σ_{BH}, as well as its derivatives, by means of numerical integration. The next three expressions are then calculated using Simpson's method:

$$\sigma_{\mathrm{BH}}(T) = \sigma - \int_0^\sigma \exp\left(-\frac{u^M}{kT}\right)dr, \tag{39}$$

$$\frac{d\sigma_{\mathrm{BH}}(T)}{dT} = \int_0^\sigma \left(\frac{u^M}{kT^2}\exp\left(-\frac{u^M}{kT}\right)\right)dr, \tag{40}$$

$$\frac{d^2\sigma_{\mathrm{BH}}(T)}{dT^2} = \int_0^{\sigma} \left(-2\frac{u^M}{kT^3}\exp\left(-\frac{u^M}{kT}\right) + \left(\frac{u^M}{kT^2}\right)^2 \exp\left(-\frac{u^M}{kT}\right)\right) dr. \quad (41)$$

A comparison between the two methods discussed above (numerical integrations and parametrization) is illustrated in Fig. 1.

IV. RESULTS AND DISCUSSION

According to the model proposed in this work, a nonassociating fluid needs five molecular parameters to be fully described: the number of segments in the chain m_s, the diameter of the segments σ, the depth of the attractive term of the potential ε/k, and the shape of the potential characterized by λ_2 (repulsive part) and λ_1 (attractive part). Therefore, the model can now account for the possibility of having different repulsive interactions between the segments in the molecule, which provides a significant improvement in the treatment of intermolecular forces involved in real substances. Moreover, since the chain term is evaluated using the cavity function of the hard-core Mie potential, it is clear that the thermodynamics of long-chain fluids will be strongly influenced by the way repulsive interactions will be modeled, i.e., by the value of the exponent λ_2. In order to emphasize the usefulness of this extra pure-component parameter, the equation of state is applied first to the *n*-alkane series (from methane to *n*-hexatriacontane), so that only repulsion-dispersion interactions have to be considered.

Before presenting the results on phase equilibria and derivative properties obtained with SAFT-VR Mie EOS, we first examine two fitting procedures and explain the relevance of the inclusion of speed of sound data (fitting procedure 2) in order to improve the optimization of the parameter λ_2. To evaluate the accuracy of the SAFT-VR Mie EOS, we take the predictions of the SAFT-VR SW (Ref. 11) as a reference since both equations are derived from the same theoretical treatment. The physical meaning of the intermolecular potential parameters obtained for *n*-alkanes will be discussed in Sec. IV D

A. Fitting procedures

Since we are dealign with *n*-alkanes, only dispersion forces have to be considered so that the value $\lambda_1=6$ is fixed. As for the parameter m_s, McCabe and Jackson[20] showed that a good description of the phase equilibrium of heavy *n*-alkanes was obtained using the simple empirical relationship: $m_s=1+(C-1)/3$.[29,30] Thus, only three parameters, $\sigma, \varepsilon/k$, and λ_2, need to be fitted to experimental data.

Because our goal is to model phase equilibrium as well as condensed liquid-phase properties, two different fitting procedures were tested. The first one consists in fitting the parameters to vapor pressure and saturated liquid density experimental data.[31] In this case two functions are defined:

$$f_{1,\mathrm{VLE}}(\sigma,\varepsilon,\lambda_2) = \sum_{i=1}^{\mathrm{N_{1,VLE}}} \left[\frac{P_{i,\mathrm{sat}}^{\mathrm{exp}} - P_{i,\mathrm{sat}}^{\mathrm{calc}}}{P_{i,\mathrm{sat}}^{\mathrm{exp}}} \right]^2, \quad (42)$$

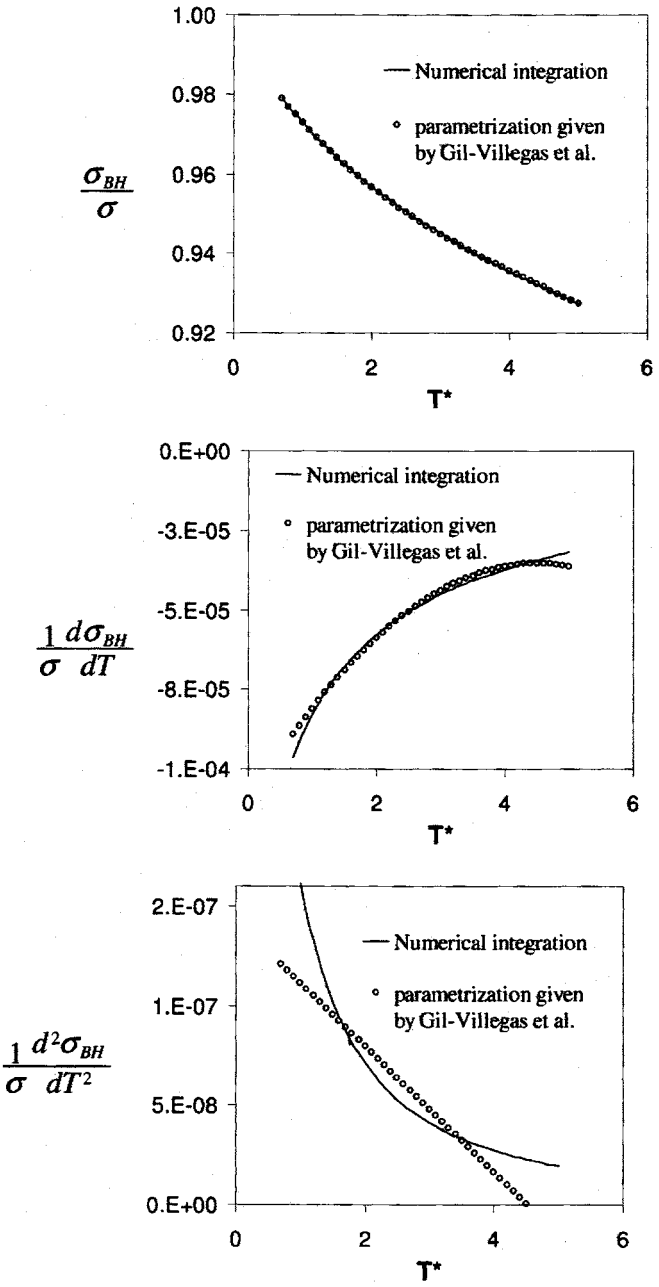

FIG. 1. Comparison of the numerical calculations (solid line) of the hard-core temperature-dependent diameter (Ref. 18) with the third-order polynomial form (circles) given by Gil-Villegas *et al.* (Ref. 11).

$$f_{2,\mathrm{VLE}}(\sigma,\varepsilon,\lambda_2) = \sum_{i=1}^{N_{2,\mathrm{VLE}}} \left[\frac{\rho_{i,\mathrm{sat}}^{\mathrm{exp}} - \rho_{i,\mathrm{sat}}^{\mathrm{calc}}}{\rho_{i,\mathrm{sat}}^{\mathrm{exp}}} \right]^2. \quad (43)$$

A Levenberg-Marquardt[19] algorithm was used to minimize the following objective function:

$$\mathrm{Min}\ 1 = w_{1,\mathrm{VLE}} f_{1,\mathrm{VLE}} + w_{2,\mathrm{VLE}} f_{2,\mathrm{VLE}}. \quad (44)$$

The weight factors $w_{1,\mathrm{VLE}}$ and $w_{2,\mathrm{VLE}}$ were set to values that fulfill the condition that $N_{i,\mathrm{VLE}} w_{i,\mathrm{VLE}}$ are constant, adopting the same value for each property ($i=1;2$). This method is referred to as procedure 1.

However, since it turns out that other versions of SAFT fail to yield good estimations for the isothermal compressibility in the condensed liquid phase (at least for *n*-alkanes),

TABLE IV. SAFT-VR Mie molecular parameters for *n*-hexane, *n*-pentadecane, and *n*-hexatriacontance obtained using fitting procedures 1 and 2. The relation $m_s=1+(C-1)/3$ is used to fix the parameter m_s.

Substance	Procedure	m_s	σ (Å)	(ε/k) (K)	λ_2
C_6H_{14}	1	2.67	4.1439	241.12	9.8167
	2	2.67	4.1344	234.4	9.5037
$C_{15}H_{32}$	1	5.67	4.2365	260.37	9.7044
	2	5.67	4.236	263.89	9.8773
$C_{36}H_{74}$	1	12.67	4.2335	236.76	8.5689
	2	12.67	4.2781	282.47	10.287

we propose here an extended fitting procedure based on a minimization of properties along the vapor-liquid equilibrium line and on the liquid phase in the one-phase region. Then the following two functions are defined:

$$f_{1,\mathrm{L}}(\sigma,\varepsilon,\lambda_2)=\sum_{i=1}^{N_{1,L}}\left[\frac{\rho_{i,\mathrm{liq}}^{\mathrm{exp}}-\rho_{i,\mathrm{liq}}^{\mathrm{calc}}}{\rho_{i,\mathrm{liq}}^{\mathrm{exp}}}\right]^2, \tag{45}$$

$$f_{2,\mathrm{L}}(\sigma,\varepsilon,\lambda_2)=\sum_{i=1}^{N_{2,\mathrm{VLE}}}\left[\frac{u_{i,\mathrm{liq}}^{\mathrm{exp}}-u_{i,\mathrm{liq}}^{\mathrm{calc}}}{u_{i,\mathrm{liq}}^{\mathrm{exp}}}\right]^2, \tag{46}$$

where ρ_{liq} and c_{liq} are the experimental density and speed of sound data[32–42] of the compressed liquid phase, respectively. In this case the objective function to minimize is the following weighted sum of the four functions defined above:

$$\mathrm{Min}\ 2=w_{1,\mathrm{VLE}}f_{1,\mathrm{VLE}}+w_{2,\mathrm{VLE}}f_{2,\mathrm{VLE}}+w_{1,\mathrm{L}}f_{1,\mathrm{L}}+w_{2,\mathrm{L}}f_{2,\mathrm{L}}. \tag{47}$$

Several values for the different weight factors $w_{1,\mathrm{VLE}}, w_{2,\mathrm{VLE}}, w_{1,\mathrm{L}}$, and $w_{2,\mathrm{L}}$ were tested, and it turned out that a good balance between accuracies of the different estimated properties was obtained imposing the condition $N_{i,\mathrm{VLE}}w_{i,\mathrm{VLE}}=2N_{i,L}w_{i,L}$ for $i=1, 2$. This method is referred to as procedure 2.

It is important to note that the speed of sound data are used instead of isothermal compressibility. Indeed, since the latter property is actually the predominant term in the calculation of the speed of sound, and since experimental data on the speed of sound are easier to determine, it is clear that this choice will make this method more useful. Moreover, the interest in adding the speed of sound to the fitting procedure is that their values are known with an excellent precision even at high-pressure and temperature conditions.

The fitting procedures 1 and 2 were tested, and fitted parameter values for some molecules of the *n*-alkanes series are reported in Table IV. It can be noticed that the parameter λ_2 varies significantly depending on the method selected. The difference between both methods is illustrated in Table V, where the AAD (%) on the saturation curve, density, and speed of sound in the condensed liquid phase for *n*-hexane (C_6), *n*-pentadecane (C_{15}), and *n*-hexatriacontane (C_{36}) with both sets of molecular parameters are reported. It is reassuring to find out that the use of Mie[9] potentials together with an extended fitting procedure allows a great improvement of the speed of sound estimation in the condensed liquid phase, while keeping an accurate description of the vapor-liquid equilibrium. Furthermore, it appears clearly that the correct determination of molecular parameters of the SAFT-VR Mie requires the inclusion of compressibility (or speed of sound) data in the parameter fitting, and hence, the application of procedure 2. As a consequence, all molecular parameters for *n*-alkanes were determined using the latter approach (Table VI), and their physical meaning will be discussed in Sec. IV D.

B. Phase equilibria of *n*-alkanes

The vapor-liquid equilibrium of *n*-alkanes (from methane to *n*-hexatriacontane), as predicted using the parameters obtained from the fitting procedure 2, is shown in Figs. 2–5. The plots show that SAFT-VR Mie EOS predicts accurately the phase envelope for $0.45<T_R<0.9 (T_R=T/T_C)$, for a wide range of chain lengths, although it overestimates the critical

TABLE V. Comparison between fitting procedures 1 and 2 using the parameters reported in Table IV.

		Vapor-liquid equilibrium			Condensed liquid phase				
		AAD (%)			AAD (%)				
Substance	Procedure	ρ_{sat}	P_{sat}	T_R range	$\rho(T,P)$	$c(T,P)$	T_R range	P_R range	Reference
C_6H_{14}	1	0.63	3.44	0.45–0.9	0.64	2.21	0.57–0.74	0.04–49.6	31 and 32
	2	0.58	3.77	0.45–0.9	0.24	2.21	0.57–0.75	0.04–49.7	
$C_{15}H_{32}$	1	0.46	1.22	0.45–0.9	0.49	2.92	0.41–0.54	0.07–101.4	31–33
	2	0.39	3.08	0.45–0.9	0.60	2.70	0.41–0.55	0.07–101.5	
$C_{36}H_{74}$	1	0.43	6.86	0.45–0.9	2.99	14.00	0.41–0.46	0.15–220.6	31–36
	2	1.19	17.69	0.45–0.9	1.17	2.75	0.41–0.47	0.15–220.7	

TABLE VI. SAFT-VR Mie molecular parameters for the *n*-alkanes series obtained using fitting procedure 2. The relation $m_s=1+(C-1)/3$ is used to fix the parameter m_s.

Substance	m_s	σ (Å)	(ε/k) (K)	λ_2
CH_4	1	3.7332	152.18	12
C_2H_6	1.33	3.8741	176.76	8.8
C_3H_8	1.67	3.9898	194.75	8.8767
C_4H_{10}	2	4.0593	212.44	9.1471
C_5H_{12}	2.33	4.11	226.87	9.4397
C_6H_{14}	2.67	4.1344	234.4	9.5037
C_7H_{16}	3	4.1642	242.9	9.6477
C_8H_{18}	3.33	4.1798	246.73	9.6941
C_9H_{20}	3.67	4.1922	252.58	9.806
$C_{10}H_{22}$	4	4.2106	256.07	9.835
$C_{11}H_{24}$	4.33	4.2188	259.34	9.892
$C_{12}H_{26}$	4.67	4.2235	261.25	9.9107
$C_{13}H_{28}$	5	4.2373	262.46	9.9201
$C_{14}H_{30}$	5.33	4.2342	264.45	9.9012
$C_{15}H_{32}$	5.67	4.236	263.89	9.8773
$C_{16}H_{34}$	6	4.2407	266.26	9.9202
$C_{17}H_{36}$	6.33	4.244	267.83	9.9263
$C_{18}H_{38}$	6.67	4.2444	269.84	10.001
$C_{19}H_{40}$	7	4.2466	268.87	9.9263
$C_{20}H_{42}$	7.33	4.2507	271.36	10
$C_{22}H_{46}$	8	4.2585	273.34	9.9954
$C_{23}H_{48}$	8.33	4.2664	275.8	10.091
$C_{24}H_{50}$	8.67	4.2702	276.42	10.125
$C_{28}H_{58}$	10	4.2648	279	10.152
$C_{36}H_{74}$	12.67	4.2781	282.47	10.287

temperature and pressure. This last effect is, in fact, a common feature to all analytical equations of state, since they exhibit a classical behavior even in the critical region. However, if the main interest were the critical behavior, McCabe and Kiselev[13,15] showed that this problem may be overcome by combining the original SAFT-VR EOS with the crossover technique developed by Kiselev.[14] The resulting equation, the so-called SAFT-VRX, provides then a precise represen-

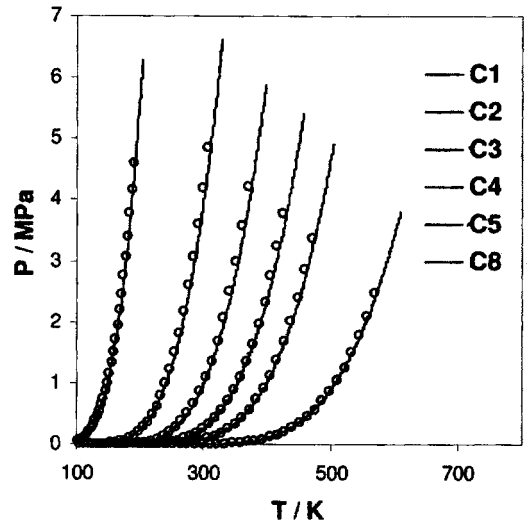

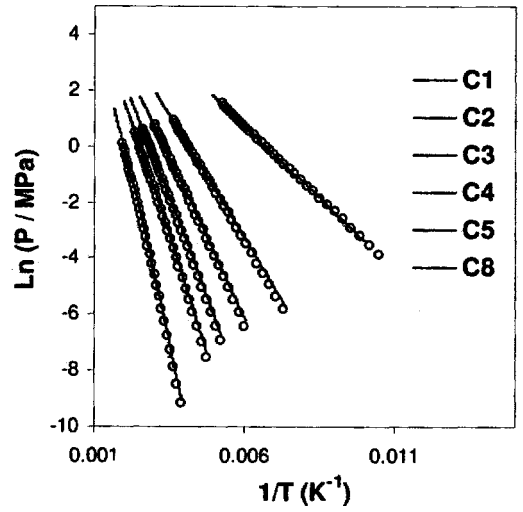

FIG. 3. Vapor pressures for light alkanes. Comparison of DIPPR correlations (Ref. 31) (circles) with calculation results of SAFT-VR Mie (continuous curves).

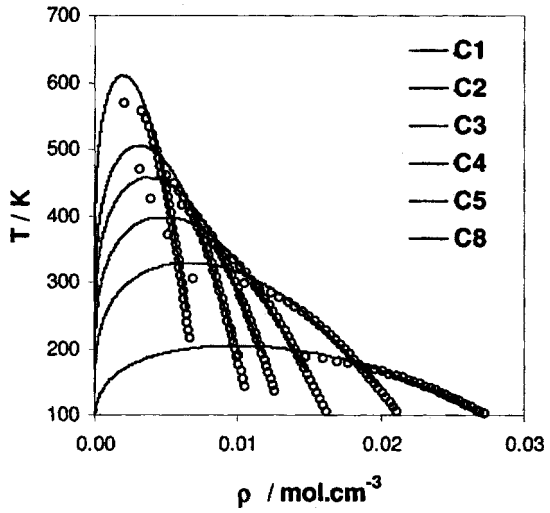

FIG. 2. Coexistence densities for light alkanes. Comparison of DIPPR correlations (Ref. 31) (circles) with calculation results of SAFT-VR Mie (continuous curves).

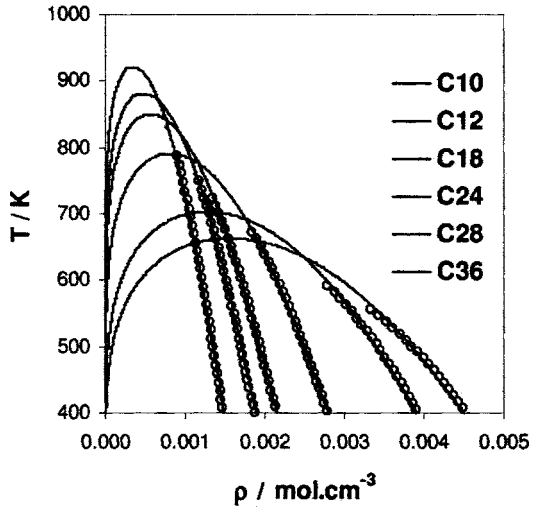

FIG. 4. Coexistence densities for heavy *n*-alkanes. Comparison of DIPPR correlations (Ref. 31) (circles) with calculation results of SAFT-VR Mie (continuous curves).

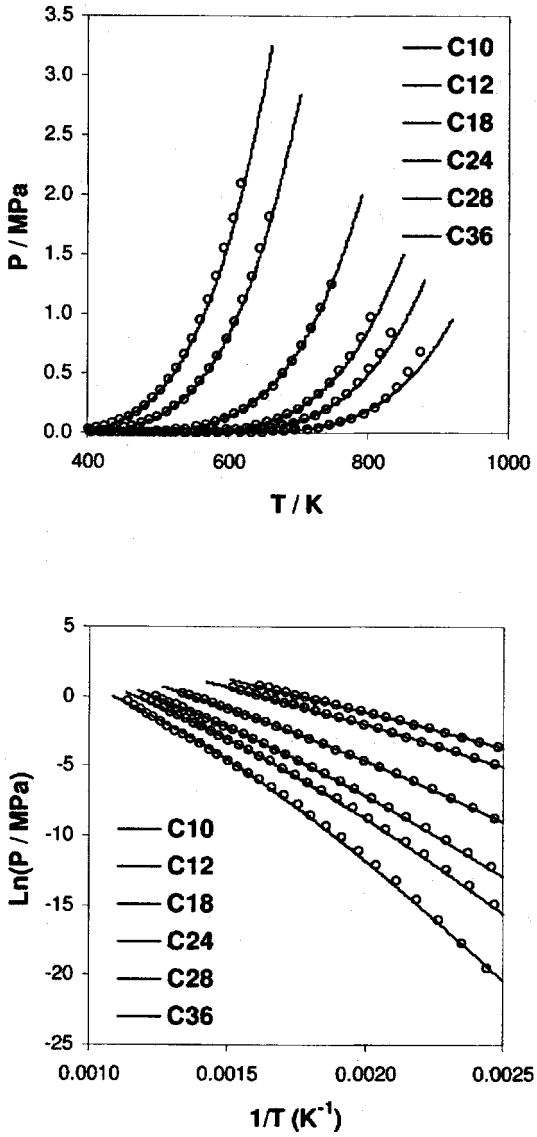

FIG. 5. Vapor pressures for heavy *n*-alkanes. Comparison of DIPPR correlations (Ref. 31) (circles) with calculation results of SAFT-VR Mie (continuous curves).

tation of the critical region while keeping the regular thermodynamic behavior of the original SAFT-VR formulation far from the critical region.

In order to evaluate the accuracy of the SAFT-VR Mie equation of state, a comparison with the SAFT-VR SW,[11] with the original parameters presented by McCabe and Jackson,[20] is presented in Table VII. From this comparison, the conclusion is that the use of Mie[9] potentials provides a slight improvement for vapor pressures and saturated liquid densities. It should be noted as well that these results are obtained without fitting exclusively on saturated properties, as was done by McCabe and Jackson[20] However, the equation seems to be less accurate at temperatures close to the triple point for light alkanes up to *n*-pentane. This may be due to the fact that this region corresponds to lower values of $T^*(T^*=Tk/\varepsilon)$, where the perturbation theory approximation is less precise. This feature is illustrated in Table VIII, where the AAD (%) on the saturation curve for two different ranges of reduced temperature ($T_R=T/T_C$) are reported: $0.45<T_R<0.9$ and $0.6<T_R<0.9$.

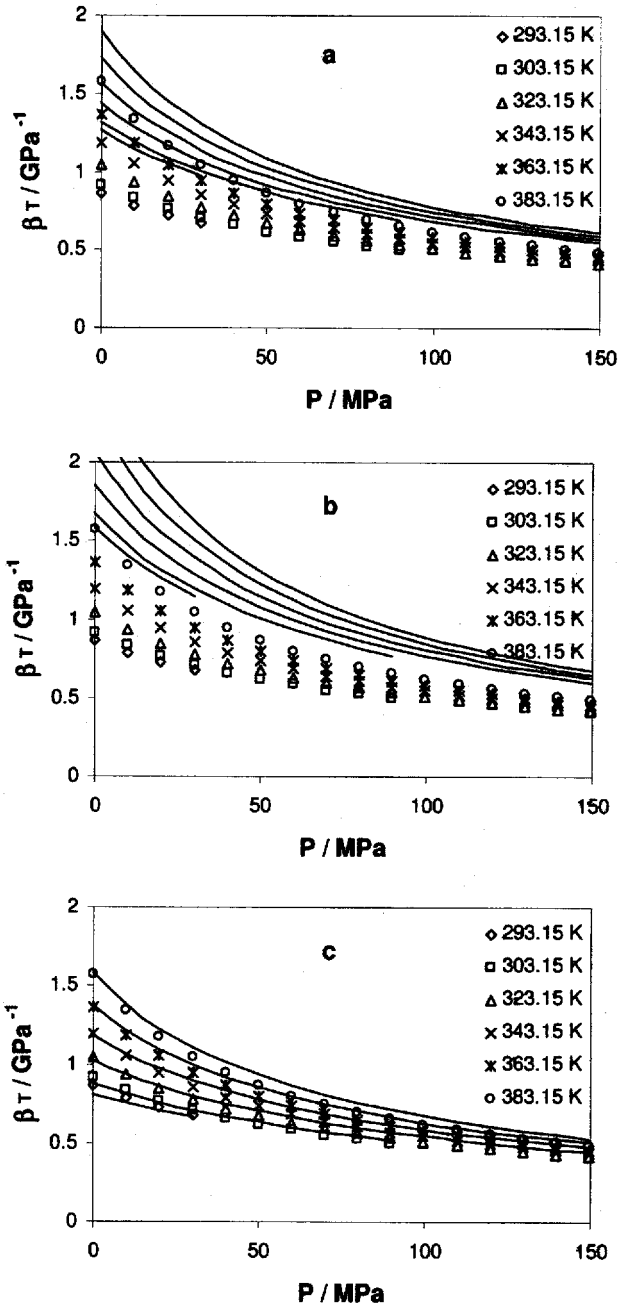

FIG. 6. Isothermal compressibility (β_T) of *n*-pentadecane. Comparison of experimental data (Ref. 33) (points) with calculation results (curves) of (a) SAFT-VR SW (Ref. 11) [with the parameters derived by McCabe and Jackson (Ref. 20)], (b) SAFT-VR LJC (Ref. 12) (with the parameters reported in Table I), and (c) SAFT-VR Mie.

C. Derivative properties of *n*-alkanes

In order to test the EOS in the compressed liquid region, density, speed of sound (properties included in the fitting procedure), isothermal compressibility, isobaric thermal expansivity, and isobaric heat capacity (predicted properties) were estimated and compared with available experimental data for long-chain *n*-alkanes. As before, in order to provide a test of ability of the SAFT-VR Mie, the results are compared with the SAFT-VR SW.[11] Table IX compares both equations in the calculations of densities and isothermal compressibilities for *n*-hexane (C_6), *n*-pentadecane (C_{15}), and *n*-hexatriacontane (C_{36}). It can be noticed that while

TABLE VII. Vapor-liquid equilibrium for *n*-alkanes. Comparison of DIPPR correlations (Ref. 31) with SAFT-VR SW (Ref. 11) [using the parameters derived by McCabe and Jackson (Ref. 20)] and SAFT-VR Mie calculations. The temperature range considered is $0.45 < T_R < 0.9$.

	SAFT-VR SW		SAFT-VR MIE		
	AAD (%)		AAD (%)		
Substance	ρ_{sat}	P_{sat}	ρ_{sat}	P_{sat}	Reference
CH_4	0.64	0.69	1.02	1.33	31
C_2H_6	1.09	2.22	0.59	8.00	31
C_3H_8	1.24	4.44	0.83	7.80	31
C_4H_{10}	0.9	3.68	0.71	5.80	31
C_5H_{12}	1.1	5.17	0.62	5.08	31
C_6H_{14}	0.91	3.37	0.58	3.77	31
C_7H_{16}	0.83	4.49	0.65	3.42	31
C_8H_{18}	0.76	4.54	0.56	4.12	31
C_9H_{20}	0.69	6.01	0.54	2.28	31
$C_{10}H_{22}$	3.72	47.4	0.61	2.02	31
$C_{11}H_{24}$	0.55	6.84	0.53	2.95	31
$C_{12}H_{26}$	1.24	6.09	0.52	1.70	31
$C_{13}H_{28}$	0.81	4.44	0.67	3.52	31
$C_{14}H_{30}$	1.49	8.49	0.38	2.17	31
$C_{15}H_{32}$	0.99	9.38	0.39	3.08	31
$C_{16}H_{34}$	0.77	5.85	0.64	2.42	31
$C_{17}H_{36}$	0.5	15.02	0.39	2.43	31
$C_{18}H_{38}$	1.35	3.5	0.4	2.96	31
$C_{19}H_{40}$	0.5	4.6	0.38	2.90	31
$C_{20}H_{42}$	0.48	5.34	0.4	3.83	31
$C_{22}H_{46}$	1.71	55.73	0.56	10.53	31
$C_{23}H_{48}$	2.42	58.22	0.41	7.11	31
$C_{24}H_{50}$	0.56	8.13	0.37	8.05	31
$C_{28}H_{58}$	0.53	9.86	0.47	10.84	31
$C_{36}H_{74}$	1.14	51.19	1.19	17.69	31

TABLE VIII. Vapor-liquid equilibrium for some light alkanes for two different ranges of temperature. Comparison of DIPPR correlations (Ref. 31) with SAFT-VR Mie calculations.

	T_R (0.45–0.9)		T_R (0.6–0.9)		
	AAD (%)		AAD (%)		
Substance	ρ_{sat}	P_{sat}	ρ_{sat}	P_{sat}	Reference
C_2H_6	0.59	8.00	0.61	3.24	31
C_3H_8	0.83	7.80	0.91	2.80	31
C_4H_{10}	0.71	5.80	0.92	2.88	31
C_5H_{12}	0.62	5.08	0.74	1.45	31

TABLE IX. Density and isothermal compressibility of the condensed liquid phase. Comparison of experimental data with SAFT-VR SW (Ref. 11) [using the parameters derived by McCabe and Jackson (Ref. 20)] and SAFT-VR Mie calculations.

			SAFT-VR SW		SAFT-VR MIE		
			AAD (%)		AAD (%)		
Substance	T_R range	P_R range	$\rho(T,P)$	$\beta_T(T,P)$	$\rho(T,P)$	$\beta_T(T,P)$	Reference
C_6H_{14}	0.57–0.74	0.04–49.6	0.49	12.31	0.24	4.11	32
$C_{15}H_{32}$	0.41–0.54	0.07–101.4	1.18	32.39	0.60	5.90	33
$C_{36}H_{74}$	0.41–0.46	0.15–220.6	2.3	21.63	1.17	6.22	36

TABLE X. Isobaric heat capacity (C_P) and residual heat capacity (ΔC_P) of the condensed liquid phase. Comparison of experimental data with calculation results of SAFT-VR SW (Ref. 11) [using the parameters derived by McCabe and Jackson (Ref. 20)] and SAFT-VR Mie.

Substance	T range (K)	P range (MPa)	SAFT-VR SW AAD (%)		SAFT-VR MIE AAD (%)		Reference
			$C_P(T,P)$	$\Delta C_P(T,P)$	$C_P(T,P)$	$\Delta C_P(T,P)$	
C_6H_{14}	298.15–403.15	10–100	6.72	28.7	5.40	22.8	43
$C_{11}H_{24}$	313.15–373.15	0.1–100	7.47	34.8	6.34	29.4	44
$C_{12}H_{26}$	313.15–373.15	0.1–100	8.07	37.3	6.78	31.2	44
$C_{13}H_{28}$	313.15–373.15	0.1–100	8.72	40.3	7.01	32.2	45
$C_{15}H_{32}$	313.15–373.15	0.1–100	8.63	39.7	7.25	33.3	46

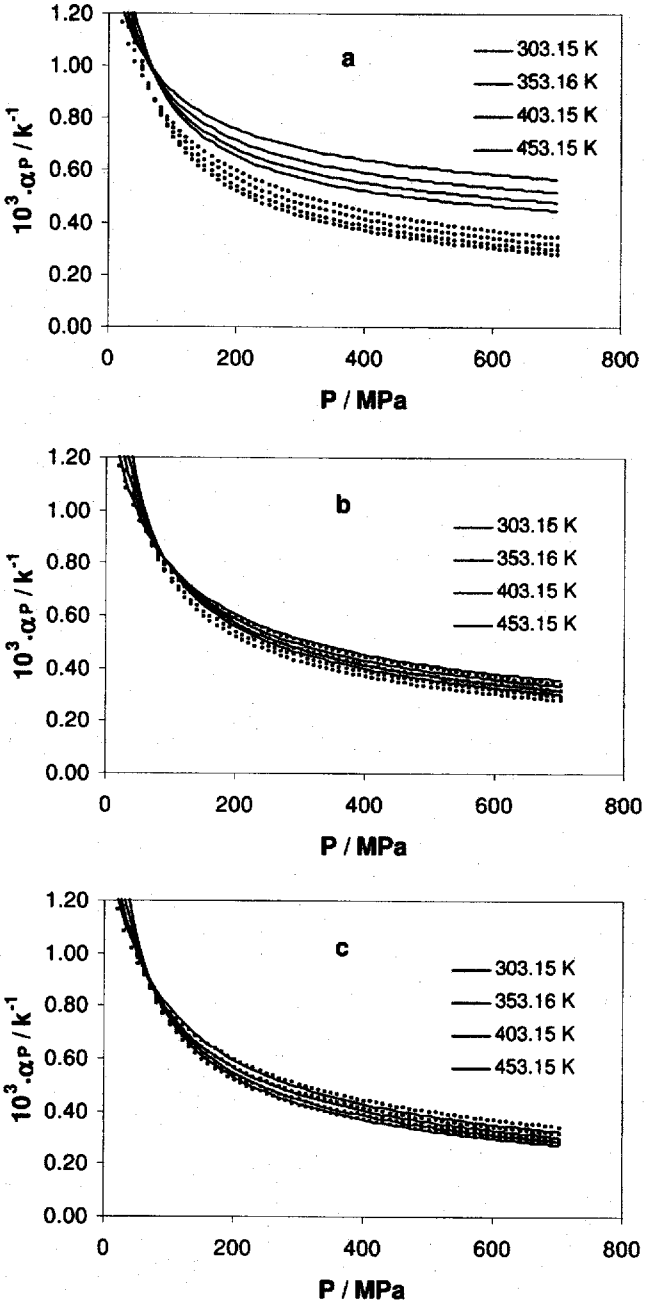

FIG. 7. Isobaric thermal expansivity (α_P) of *n*-hexane. Comparison of experimental data (Ref. 43) (points) with calculation results (curves) of (a) SAFT-VR SW (Ref. 11) [with the parameters derived by McCabe and Jackson (Ref. 20)], (b) SAFT-VR LJC (Ref. 12) (with the parameters reported in Table I), and (c) SAFT-VR Mie.

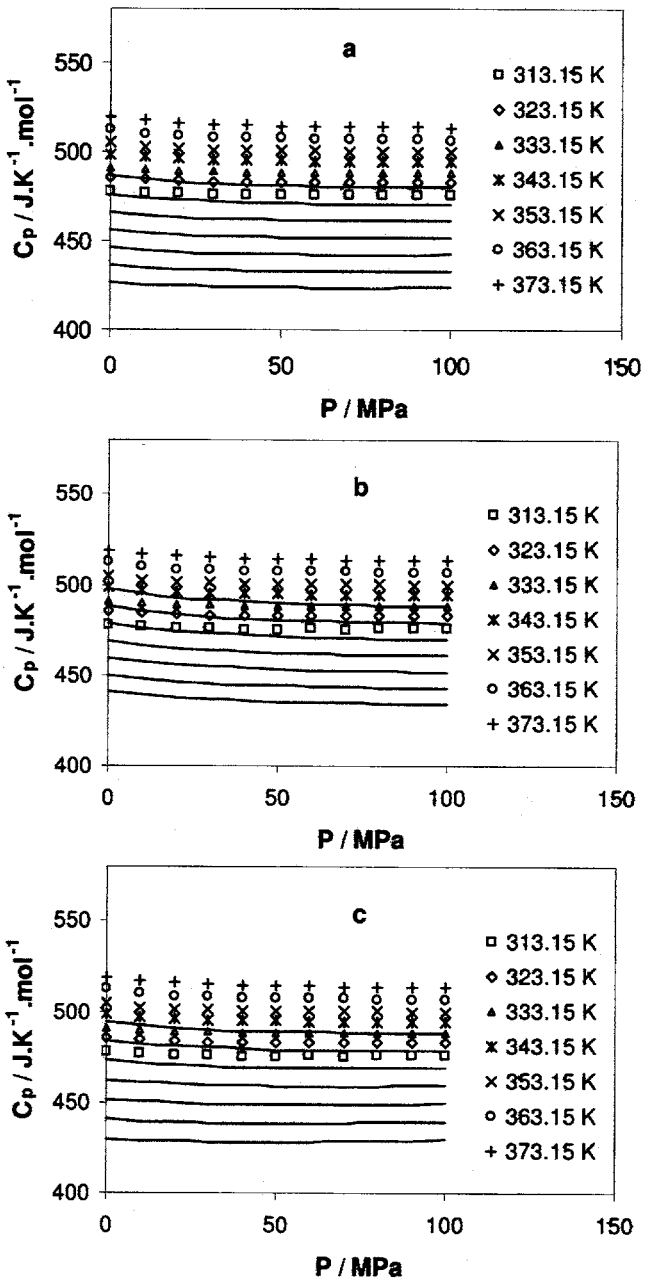

FIG. 8. Isobaric heat capacity (C_p) of *n*-pentadecane. Comparison of experimental data (Ref. 46) (points) with calculation results (curves) of (a) SAFT-VR SW (Ref. 11) [with the parameters derived by McCabe and Jackson (Ref. 20)], (b) SAFT-VR LJC (Ref. 12) (with the parameters reported in Table I), and (c) SAFT-VR Mie.

TABLE XI. Speed of sound (u) of the condensed liquid phase for some n-alkanes from n-hexane to n-hexatriacontane. Comparison of experimental data with calculation results of SAFT-VR SW (Ref. 11) [using the parameters derived by McCabe and Jackson (Ref. 20)] and SAFT-VR Mie.

			SAFT-VR SW	SAFT-VR MIE	
Substance	T range (K)	P range (MPa)	AAD (%) $u(T,P)$	AAD (%) $u(T,P)$	Reference
C_6H_{14}	293.15–373.15	0.1–150	4.71	2.21	32
$C_{10}H_{22}$	303.15–413.15	0.1–60	13.11	2.46	33
$C_{15}H_{32}$	293.15–383.15	0.1–150	12.63	2.70	33
$C_{20}H_{42}$	323.15–393.15	0.1–150	15.93	2.62	37
$C_{24}H_{50}$	333.15–393.15	0.1–150	16.47	2.40	38
$C_{36}H_{74}$	363.15–403.15	0.1–150	10.16	2.75	36

SAFT-VR SW (Ref. 11) fails to describe the isothermal compressibility, SAFT-VR Mie gives excellent predictions and no significant deterioration is found with increasing chain length (Fig. 6). This shows the relevance of using a variable repulsive part in the intermolecular potential since the parameter λ_2 was found to vary significantly from n-hexane to n-hexatriacontane.

Another severe test for an EOS is the estimation of the intersection of isotherms of the isobaric thermal expansivity, because to achieve this the EOS must describe with great accuracy the $P(v,T)$ function, as well as its first temperature and volume partial derivatives. Calculations of the isobaric thermal expansivity of n-hexane with SAFT-VR SW,[11] SAFT-VR LJC,[12] and SAFT-VR Mie are compared with literature-correlated data[43] in Fig. 7. The AAD of the differences between SAFT-VR Mie and the correlated data over the whole temperature and pressure range is 2.2%, while SAFT-VR SW yields 37.3% and SAFT-VR LJC 5.6%. Moreover, SAFT-VR Mie reproduces with a good accuracy the cited crossing point between isotherms. This emphasizes the consistency of the fitting procedure used because this property was not included in the regression of the parameters.

The second-order derivative of the Helmholtz free energy was also studied by calculations of isobaric heat capacities. Table X reports the AAD (%) in isobaric heat capacity for n-hexane,[36] n-undecane,[44] n-dodecane,[37] n-tridecane,[45] and n-pentadecane (Ref. 46) as functions of temperature and pressure for SAFT-VR SW (Ref. 11) and SAFT-VR Mie. From these results, the conclusion that no significant improvement for this property is found by the inclusion of Mie[9] potentials within the SAFT-VR approach can be stressed. This result is probably due to the fact that although the hard-sphere and chain terms contribute to the second-order derivative [through the temperature-dependent diameter[18] $\sigma_{BH}(T)$], it is the dispersion term who plays a dominant role, and hence, a better description of this property would require probably the calculation of higher-order perturbation terms. A comparative plot of the isobaric heat capacity of n-pentadecane is shown in Fig. 8.

Finally, the SAFT-VR Mie EOS was tested against the speed of sound data from n-hexane to n-hexatriacontane (Fig. 9) and the AAD (%) for some of these alkanes are listed in Table XI. No deterioration of the results is observed up to n-hexatriacontane, which is very gratifying since the speed

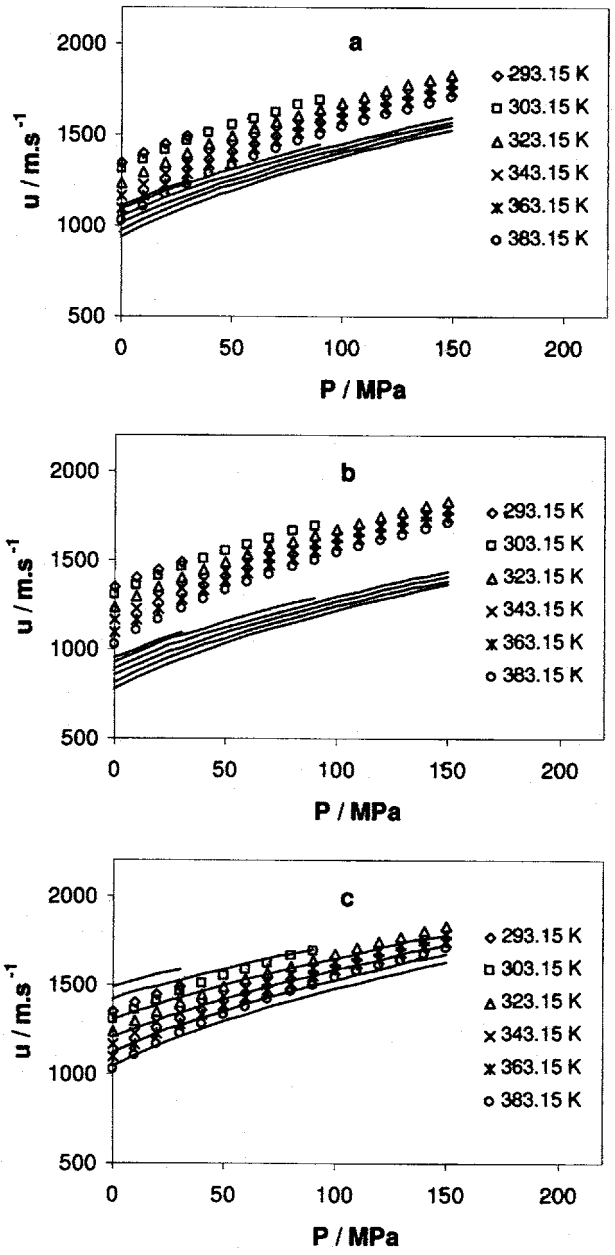

FIG. 9. Speed of sound (u) of n-pentadecane. Comparison of experimental data (Ref. 33) (points) with calculation results (curves) of (a) SAFT-VR SW (Ref. 11) [with the parameters derived by McCabe and Jackson (Ref. 20)], (b) SAFT-VR LJC (Ref. 12) (with the parameters reported in Table I), and (c) SAFT-VR Mie.

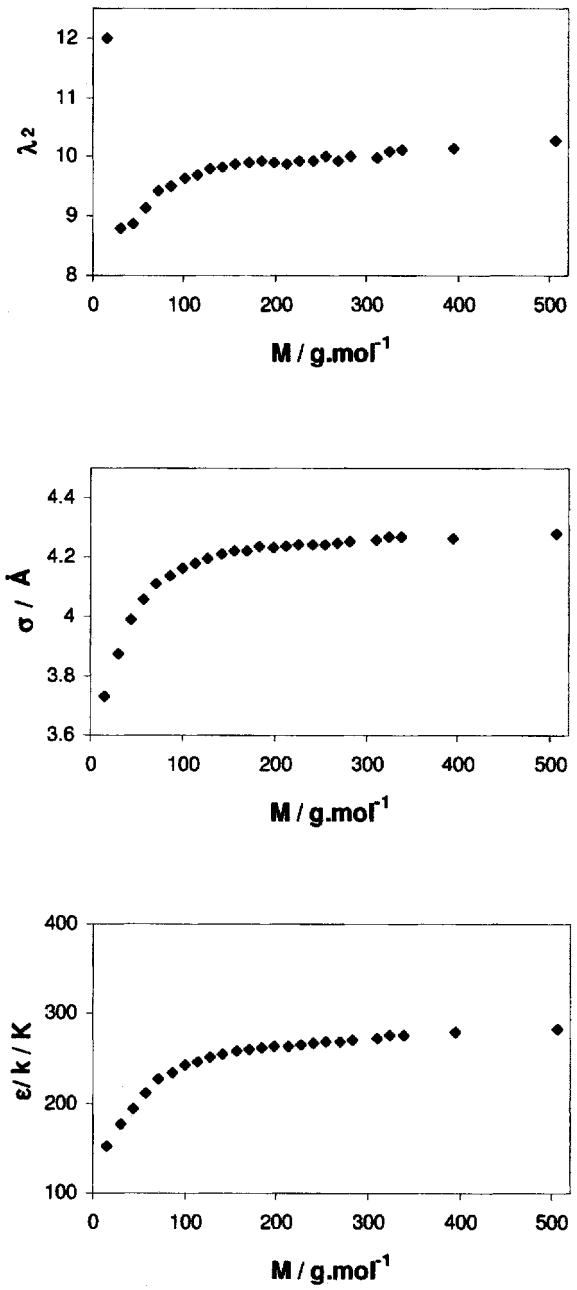

FIG. 10. Pure-component parameters of the SAFT-VR Mie equation of state for the *n*-alkanes series as a function of molar mass.

of sound calculation involves all the previous thermophysical properties (density, isothermal compressibility, isobaric thermal expansivity, isobaric heat capacity).

D. Physical meaning of the intermolecular potential parameters

It should be noted here that this study on *n*-alkanes was intended as an example to show the usefulness of the inclusion of a variable repulsive part in the intermolecular potential. Furthermore, the results reported demonstrate that an accurate description of the repulsive interaction is of major importance to predict accurately the compressibility of the condensed liquid phase. Hence, as nonlinear fitting can lead to different sets of parameters, it is clear that parameters with real physical meaning will be obtained if compressibility data are included in the fitting procedure.

Figure 10 shows the molecular parameters obtained as a function of molecular mass. The regular trend observed for each parameter, $\lambda_2, \sigma, \varepsilon/k$, emphasizes their physical meaning. Indeed, every parameter value increases with chain length for the shorter members of the series, and later converges to constant values as the segment number increases. This trend may be explained by the fact that for long-chain *n*-alkanes the ratio of CH_3 groups versus CH_2 becomes negligible, so that the structure of these molecules is not essentially changed by the addition of new CH_2 groups.

As could be expected *a priori*, methane (modeled as a single CH_4 unit) turns out to be a particular case since we obtained for the repulsive part $\lambda_2=12$, the upper limiting value in the range of definition of this parameter ($3<\lambda_2 \leqslant 12$, see Sec. III B). Thus, another parametrization of the equation for a broader range seems to be necessary in order to determine the correct value of the repulsive exponent for this molecule.

Finally, it should be noted that $m_s\lambda_2, m_s\varepsilon/k$, and $m_s\sigma^3$ can be correlated with a linear relationship as a function of molecular weight (M) allowing the prediction of parameters for heavier compounds, for which no experimental data exist, extrapolating the described method in a purely predictive way.

$$m_s\sigma^3 = 1.9119M + 24.2251, \tag{48}$$

$$m_s\varepsilon/k = 6.9946M + 21.5765, \tag{49}$$

$$m_s\lambda_2 = 0.2470M + 3.9612. \tag{50}$$

V. CONCLUSIONS

A modified SAFT-VR EOS (SAFT-VR Mie) has been presented using the Mie *m-n* family of potentials. The essence of this work was to show the importance of improving the description of repulsion interactions between the monomer segments constituting the molecules in order to enhance the SAFT model performance, especially in the calculation of derivative properties (isothermal compressibility, isobaric thermal expansivity, speed of sound).

The equation of state was applied to the *n*-alkane series with the aim of capturing the thermophysical influence of increasing chain length. When compared with classical equations of state and other SAFT versions (PC-SAFT, SAFT-VR SW, and SAFT-VR LJC), which fail to yield good estimations on isothermal compressibilities and speed of sound, the SAFT-VR Mie model was found to give an accurate description of both vapor-liquid equilibrium and derivative properties.

It is important to mention that the choice of the SAFT-VR approach was motivated by the fact that this theory allows the modification of the intermolecular potential model while keeping simple and compact expressions for the calculation of each contribution to the free energy. Moreover, the equation of state presented above can be easily extended

to mixtures in the framework of Galindo *et al.*[47] on SAFT-VR for square-well potential, and to associating molecules also, adopting the association expression of the SAFT (Chapman *et al.*[48]), which will be the goal of future work.

Additionally, the interest in adding density and speed of sound data of the condensed liquid phase to the classical fitting procedure has been demonstrated. This new parameter calculation method yields an excellent balance between accuracies of the different estimated properties and, at the same time, molecular parameters with a stronger physical meaning.

ACKNOWLEDGMENTS

The authors wish to acknowledge G. Jackson and A. Galindo for their encouraging comments and fruitful discussions about this work

APPENDIX A: LIST OF SYMBOLS

R=gas constant, J mol^{-1} K^{-1}
M=molar mass, g mol^{-1}
N_a=Avogadro's number
k=Boltzmann constant, J K^{-1}
m_s=number of segments per chain
r=radial distance between two segments, Å
P=pressure, Pa
V=volume, m^3
T=temperature, K
N_s=total number of spherical segments
N=total number of molecules
A=Helmholtz free energy, J
β_T=isothermal compressibility, Pa^{-1}
β_S=isentropic compressibility, Pa^{-1}
C_P=isobaric heat capacity, J K^{-1} mol^{-1}
α_P=isobaric thermal expansivity, K^{-1}
u=speed of sound, m s^{-1}
a_1=Helmholtz free energy per monomer segments of first-order perturbation term, J
a_2=Helmholtz free energy per monomer segments of second-order perturbation term, J
$u(r)$=pair potential function, J
ε=depth of pair potential, J
σ=segment diameter, 1/Å^3
λ_2=repulsive exponent of the Mie potential
λ_1=attractive exponent of the Mie potential
σ_{BH}=temperature-dependent segment diameter, Å
η=packing fraction
Z=compressibility factor
BH =property calculated using the Barker-Henderson perturbation theory
liq =property in the condensed liquid phase
sat =property at saturation condition
M=monomer reference system
calc=calculated property
exp=experimental property
mono=contribution of monomer system
Chain=contribution due to the formation of chains
Assoc=association contribution
Res=residual contribution

APPENDIX B: EQUATIONS FOR CALCULATING THE DERIVATIVE PROPERTIES USING THE SAFT-VR MIE MODEL

This section provides the expressions that were used to calculate the derivative properties: isothermal compressibility, isobarci thermal expansivity, isobaric heat capacity, isochoric heat capacity, isentropic compressibility, and speed of sound. These derivative properties are given in terms of the residual Helmholtz energy (A^{res}) and of the compressibility factor (Z) which is derived using the expression

$$Z = 1 + \eta_{BH}\left(\frac{\partial a^{res}}{\partial \eta_{BH}}\right)_T. \tag{B1}$$

Isothermal compressibility (Pa^{-1}):

$$\beta_T = \frac{1}{\eta_{BH}}\left(\frac{\partial P}{\partial \eta_{BH}}\right)_T^{-1}. \tag{B2}$$

Isobaric thermal expansivity (K^{-1}):

$$\alpha_P = \frac{1}{\eta_{BH}}\frac{(\partial P/\partial T)_\rho}{(\partial P/\partial \eta_{BH})_T}, \tag{B3}$$

with

$$\left(\frac{\partial P}{\partial T}\right)_\rho = 10^{30}\rho kT\left(\left(\frac{\partial Z}{\partial T}\right)_\rho + \frac{Z}{T}\right), \tag{B4}$$

$$\left(\frac{\partial P}{\partial \eta_{BH}}\right)_T = 10^{30}\rho kT\left(\left(\frac{\partial Z}{\partial \eta_{BH}}\right)_T + \frac{Z}{\eta_{BH}}\right). \tag{B5}$$

Residual isochoric heat capacity (J K^{-1} mol^{-1}):

$$C_V^{res} = -2RT\left(\frac{\partial a^{res}}{\partial T}\right)_\rho - RT^2\left(\frac{\partial^2 a^{res}}{\partial T^2}\right)_\rho. \tag{B6}$$

Residual isobaric heat capacity (J K^{-1} mol^{-1}):

$$C_P^{res} = C_V^{res} - R + \left(\frac{TN_a}{10^{30}\rho\eta_{BH}}\right)\frac{(\partial P/\partial T)_\rho^2}{(\partial P/\partial \eta_{BH})_T}. \tag{B7}$$

Isentropic compressibility (Pa^{-1}):

$$\beta_S = \beta_T - \frac{\alpha_P^2 T N_a}{10^{30}\rho(C_P^{id} + C_P^{res})}. \tag{B8}$$

The ideal-gas heat capacities C_p^{id} were calculated using the Planck-Einstein function fitted to experimental data (Coniglio and Daridon[49]). **Speed of sound (m s^{-1})**:

$$u = \frac{1}{\sqrt{(10^{30}\rho M/N_a)\beta_S}}. \tag{B9}$$

[1] W. G. Chapman, K. E. Gubbins, G. Jackson, and M. Radosz, Ind. Eng. Chem. Res. **29**, 1709 (1990).
[2] M. S. Wertheim, J. Stat. Phys. **35**, 19 (1984).
[3] M. S. Wertheim, J. Stat. Phys. **35**, 35 (1984).
[4] M. S. Wertheim, J. Stat. Phys. **42**, 459 (1986).
[5] M. S. Wertheim, J. Stat. Phys. **42**, 477 (1986).
[6] M. S. Wertheim, J. Chem. Phys. **85**, 2929 (1986).
[7] M. S. Wetheim, J. Chem. Phys. **87**, 7323 (1987).
[8] E. A. Müller and K. A. Gubbins, in *Equations of State for Fluids and Fluid Mixtures* (Elsevier, New York, 2000), Vol. 2, pp. 435–477.

[9] T. M. Reed and K. E. Gubbins, *Applied Statistical Mechanics* (McGraw-Hill, Tokyo, 1973).
[10] J. Gross and G. Sadowski, Ind. Eng. Chem. Res. **40**, 1244 (2001).
[11] A. Gil-Villegas, A. Galindo, P. J. Whitehead, S. J. Mills, G. Jackson, and A. N. Burgess, J. Chem. Phys. **106**, 4168 (1997).
[12] L. A. Davies, A. Gil-Villegas, and G. Jackson, Int. J. Thermophys. **19**, 675 (1998).
[13] C. McCabe and S. B. Kiselev, Fluid Phase Equilib. **219**, 3 (2004).
[14] S. B. Kiselev, Fluid Phase Equilib. **147**, 7 (1998).
[15] C. McCabe and S. B. Kiselev, Fluid Phase Equilib. **43**, 2839 (2004).
[16] J. A. Barker and D. Henderson, J. Chem. Phys. **47**, 2856 (1967).
[17] J. A. Barker and D. Henderson, J. Chem. Phys. **47**, 4714 (1967).
[18] J. A. Barker and D. Henderson, Rev. Mod. Phys. **48**, 587 (1975).
[19] D. W. Marquadt, J. Soc. Ind. Appl. Math. **11**, 431 (1963).
[20] C. McCabe and G. Jackson, Phys. Chem. Chem. Phys. **1**, 2057 (1999).
[21] D. Y. Peng and D. B. Robinson, Ind. Eng. Chem. Fundam. **15**, 59 (1976).
[22] G. Soave, Fluid Phase Equilib. **44**, 345 (1972).
[23] M. Benedict, G. R. Webb, and L. C. Rubin, J. Chem. Phys. **8**, 334 (1940).
[24] B. I. Lee and M. G. Kesler, AIChE J. **21**, 510 (1975).
[25] H. Nishiumi and S. Saïto, J. Chem. Eng. Jpn. **8**, 356 (1975).
[26] J. K. Johnson, E. A. Müller, and K. E. Gubbins, J. Chem. Phys. **98**, 6413 (1994).
[27] N. F. Carnahan and K. E. Starling, J. Chem. Phys. **51**, 635 (1969).
[28] J. K. Percus and G. J. Yevick, Phys. Rev. **110**, 1 (1958).
[29] A. L. Archer, M. D. Amos, G. Jackson, and I. A. McLure, Int. J. Thermophys. **17**, 201 (1996).
[30] G. Jackson and K. E. Gubbins, Pure Appl. Chem. **61**, 1021 (1989).
[31] T. E. Daubert and R. P. Danner, *Data Compilation Tables of Properties of Pure Compounds* (AIChE, New York, 1985); (AIChE, New York, 1986); (AIChE, New York, 1989); *Design Institute for Physical Property Data*, DIPPR 801 Tables (AIChE, New York, 1992).
[32] J. L. Daridon, B. Lagourette, and J. P. E Grolier, Int. J. Thermophys. **19**, 145 (1998).
[33] J. L. Daridon, H. Carrier, and B. Lagourette, Int. J. Thermophys. **23**, 697 (2002).
[34] J. L. Daridon, A. Lagrabette, and B. Lagourette, Phys. Chem. Liq. **37**, 137 (1999).
[35] J. L. Daridon and B. Lagourette, High Temp. - High Press. **32**, 83 (2000).
[36] S. Dutour, B. Lagourette, and J. L. Daridon, J. Chem. Thermodyn. **34**, 475 (2002).
[37] S. Dutour, J. L. Daridon, and B. Lagourette, High Temp. - High Press. **33**, 371 (2001).
[38] S. Dutour, J. L. Daridon, and B. Lagourette, J. Chem. Thermodyn. **33**, 765 (2001).
[39] J. L. Daridon, Acustica **80**, 416 (1994).
[40] J. W. M. Boelhouwer, Physica (Amsterdam) **34**, 484 (1967).
[41] A. L. Badalyan and N. F. Otpuschennikov, Izv. Akad. Nauk. SSSR, Fiz. Zemli **6**, 207 (1971).
[42] S. Dutour, J. L. Daridon, and B. Lagourette, Int. J. Thermophys. **21**, 173 (2000).
[43] S. L. Randzio, J. P. E Grolier, J. R. Quint, D. J. Eatough, E. A. Lewis, and L. D. Hansen, Int. J. Thermophys. **3**, 415 (1994).
[44] D. Bessieres, H Saint-Guirons, and J. L. Daridon, High Press. Res. **18**, 279 (2000).
[45] D. Bessieres, H. Saint-Guirons, and J. L. Daridon, J. Therm Anal. Calorim. **62**, 621 (2000).
[46] D. Bessieres, H. Saint-Guirons, and J. L. Daridon, Phys. Chem. Liq. **39**, 301 (2001).
[47] A. Galindo, L. A. Davies, A. Gil-Villegas, and G. Jackson, Mol. Phys. **93**, 241 (1998).
[48] W. G. Chapman, G. Jackson, and K. E. Gubbins, Mol. Phys. **65**, 1057 (1988).
[49] L. Coniglio and J. L. Daridon, Fluid Phase Equilib. **139**, 15 (1997).